Scaling of linear microtearing stability for a high collisionality National Spherical Torus Experiment discharge

W. Guttenfelder, J. Candy, S. M. Kaye, W. M. Nevins, R. E. Bell et al.

Citation: Phys. Plasmas **19**, 022506 (2012); doi: 10.1063/1.3685698
View online: http://dx.doi.org/10.1063/1.3685698
View Table of Contents: http://pop.aip.org/resource/1/PHPAEN/v19/i2
Published by the American Institute of Physics.

Scaling of linear microtearing stability for a high collisionality National Spherical Torus Experiment discharge

W. Guttenfelder,[1] J. Candy,[2] S. M. Kaye,[1] W. M. Nevins,[3] R. E. Bell,[1] G. W. Hammett,[1] B. P. LeBlanc,[1] and H. Yuh[4]
[1]*Princeton Plasma Physics Laboratory, Princeton, New Jersey 08543, USA*
[2]*General Atomics, San Diego, California 92186, USA*
[3]*Lawrence Livermore National Laboratory, Livermore, California 04551, USA*
[4]*Nova Photonics Inc., Princeton, New Jersey 08540, USA*

(Received 25 October 2011; accepted 12 January 2012; published online 22 February 2012)

Linear gyrokinetic simulations are performed based on a high collisionality NSTX discharge that is part of dimensionless confinement scaling studies. In this discharge, the microtearing mode is predicted to be unstable over a significant region of the plasma ($r/a = 0.5$–0.8), motivating comprehensive tests to verify the nature of the mode and how it scales with physical parameters. The mode is found to be destabilized with sufficient electron temperature gradient, collisionality, and beta, consistent with previous findings and simple theoretical expectations. Consistent with early slab theories, growth rates peak at a finite ratio of electron-ion collision frequency over mode frequency, $\nu^{e/i}/\omega \sim 1$–6. Below this peak, the mode growth rate decreases with reduced collisionality, qualitatively consistent with global confinement observations. Also, in this region, increased effective ionic charge (Z_{eff}) is found to be destabilizing. Experimental electron beta and temperature gradients are two to three times larger than the inferred linear thresholds. Increasing magnetic shear (s) and decreasing safety factor (q) are both destabilizing for ratios around the experimental values $s/q = 0.6$–1.3. Both the Z_{eff} and s/q scaling are opposite to those expected for the ETG instability offering an opportunity to experimentally distinguish the two modes. Finally, we note that the kinetic ballooning mode is found to compete with the microtearing mode at outer locations $r/a \geq 0.8$. [doi:10.1063/1.3685698]

I. INTRODUCTION

Ion thermal transport in spherical tokamaks (STs) is routinely down to neoclassical levels in the presence of sufficient $E \times B$ shear,[1–4] which occurs in strongly beam heated plasmas. However, there remains a great demand to understand the cause of anomalous electron thermal transport and its influence on confinement as it will influence the design of next generation devices.

Recent experiments show that in both the National spherical torus experiment (NSTX) (Ref. 1) and MAST (Ref. 3) spherical tokamaks, the normalized energy confinement time $\Omega \cdot \tau_E$ (where $\Omega = eB/m$ is the cyclotron frequency) has a much stronger dependence on collisionality $(\Omega\tau_E)_{ST} \sim \nu_*^{-(0.8-0.95)}$ compared to conventional tokamaks, as characterized by the ITER Physics Basis, $(\Omega\tau_E)_{H98(y,2)} \sim \nu_*^{-0.01}$.[5] Such a strong inverse scaling is favorable for the design of next generation ST devices that operate at much lower collisionality. However, it is not understood theoretically what is responsible for this unique scaling in STs. In addition, a comparison of $\Omega \cdot \tau_E$ across many different tokamaks suggests that the ν_* scaling exponent depends on the value of ν_* itself.[6] It is, therefore, unclear if the favorable ν_* scaling will hold at lower ν_*.

Linear gyrokinetic studies in STs (Refs. 7–19) have found that when the micro-tearing (MT) mode is unstable, there are regions in collisionality where it scales qualitatively consistent with the observed global confinement and local transport, i.e., linear growth rates decrease with decreasing collisionality.[3,16,19] In contrast, other modes such as ion temperature gradient and trapped electron mode (ITG/TEM) tend to be stabilized by increasing collisionality. In NSTX, there are discharges that occur where the microtearing mode instability appears to dominate over all other micro-instabilities.[17,19,20] In this paper, we study the linear properties and scaling of the MT mode for one such case, a high-ν_* NSTX discharge that is part of confinement scaling studies[1] and was recently the basis of nonlinear gyrokinetic simulations of microtearing turbulence.[20] We use it for more thorough linear analysis in an effort to understand when and where microtearing may be important in ST plasmas and to identify possible ways to experimentally discriminate it from other instabilities such as the electron temperature gradient (ETG) instability.

Some useful reviews of many features of microtearing modes in spherical tokamaks are addressed in Refs. 13–16. Microtearing modes are small scale tearing instabilities[21,22] with large toroidal (n) and poloidal (m) mode numbers. Theoretically, they are driven unstable by having an equilibrium electron temperature gradient ∇T_e projected onto helically resonant radial perturbations of magnetic field lines, δB_{mn}, with a rational value of the safety factor, $q = m/n$. The resulting parallel component of ∇T_e can drive a resonant parallel current through multiple mechanisms, such as the time-dependent thermal force[23–32] or particle trapping,[33–35] both requiring finite collisionality. The driven parallel

current reinforces δB via Ampere's law allowing instability to grow. The existence and strength of the instability should, therefore, depend on collisionality, electron beta (from Ampere's law), and the equilibrium temperature gradient. Early slab calculations[26–28] and more recent gyrokinetic tokamak simulations[15,16,19] have verified these expectations. For the high-ν_* NSTX discharge addressed in this paper, we find the thresholds in electron beta and temperature gradient are exceeded by a large margin (2–3×).

One of the distinguishing features is the peak in growth rate (γ) at finite collision frequency, which depends on the ratio of electron-ion collision frequency to mode frequency, $\nu^{e/i}/\omega$. Above this peak ($\nu^{e/i} \gg \omega$) in the so-called "semi-collisional" limit,[24] growth rates are proportional to $\sim\omega/\nu$. However, for many tokamak and ST discharges, we are often interested in the more weakly collisional range $\nu^{e/i} \leq \omega$, where growth rates increase with $\nu^{e/i}$.[23,27,28] This non-monotonic dependence of γ on $\nu^{e/i}$ has been predicted in numerous gyrokinetic simulations,[3,16,19] and it also implies a dependence on effective ionic charge (Z_{eff}) which determines the electron-ion collision frequency. For the NSTX experimental range of parameters, we find increasing Z_{eff} to be destabilizing. This is opposite to the influence on the ETG instability[36] (which is stable in this discharge) and may be used to help distinguish these two modes experimentally.

Slab theory and simulations[26–28] also predict that microtearing modes should depend non-monotonically on magnetic shear through stabilizing effects from field line bending. This scaling has not been systematically studied in tokamaks. Using a local equilibrium expansion to independently vary safety factor (q) and magnetic shear ($s = r/q \cdot dq/dr$), we find that around the experimental values in this paper (characterized by the ratio $s/q = 0.6–1.3$), increasing shear or decreasing safety factor is destabilizing. Similar to Z_{eff}, this dependence is opposite to that expected for ETG turbulence (for comparable values) offering a second experimental knob for distinguishing theoretical mode dominance.

In some NSTX experiment-based calculations, microtearing growth rates were found to be reduced by reverse shear ($s < 0$) in neutral beam injection (NBI) discharges,[17,18] consistent with the above scaling. More recently, however, a tearing parity mode approaching electron scales ($k_\theta \rho_s = 3–15$) was found in the core of RF heated discharges near zero magnetic shear $|s| < 0.1$.[37] Our systematic scans also find the microtearing instability to exist for very small magnetic shear but at ion scale wavelengths ($k_\theta \rho_s < 2$).

While high beta is expected to enhance MT modes in STs, they have also been found unstable in lower beta conventional aspect ratio tokamaks (ASDEX-Upgrade)[38–40] especially as the edge is approached. Many of the parametric scalings (ν_e, β_e, a/L_{Te}) are similar to that found in the ST, although they apparently occur at smaller wavelengths ($k_\theta \rho_s \leq 0.2$). We also note they have been predicted to be unstable in improved confinement regimes of reverse field pinch plasmas.[41] Understanding the wider scaling of the microtearing mode as investigated in this paper is, therefore, of broad interest to the magnetic confinement community.

Throughout this paper, we use the Eulerian gyrokinetic code GYRO (Ref. 42–44) for linear stability calculations as it is capable of including all necessary physics, namely multiple gyro-kinetic species, fully electromagnetic effects (shear and compressional[45]), electron pitch angle scattering, and general numerical equilibrium reconstruction.[46] It can also allow for profile variations (i.e., non flux-tube) and equilibrium flow and flow shear, although we do not include these effects in the linear calculations. For all microtearing simulations, the code is run as an initial value solver (indicated by lines with symbols). As parameters are varied, other modes can become dominant such as the kinetic ballooning mode (KBM). In many of these cases, we use the recently implemented eigenvalue solver[45] to track the additional roots in parameter space (indicated by dashed lines with no symbols), even as they become subdominant.

The remainder of this paper is organized as follows. Section II provides some details about the experimental NSTX discharge under analysis as well as linear calculations at a few locations showing the microtearing mode is the dominant instability for a substantial confining region of the plasma. In Sec. III, we present many parametric scans of the microtearing mode varying collisionality, gradients, beta, safety factor, and magnetic shear. We summarize the key results in Sec. IV, outlining the most salient features regarding interpretation of experimental observations.

II. EXPERIMENTAL PARAMETERS, LINEAR ANALYSIS, AND MODEL ASSUMPTIONS

We focus on NSTX discharge 120968 ($B_T = 0.35$ T, $I_p = 0.7$ MA, $R/a = 0.82/0.62$ m, and $P_{NBI} = 4$ MW) with line-averaged density $\bar{n}_e = 5.4 \times 10^{19}$ m^{-3}, peak temperatures $T_e(0) \approx T_i(0) = 0.85$ keV, volume-averaged toroidal beta $\beta_{tor} = 19\%$, boundary surface elongation $\kappa = 2.0$, and lower/upper triangularity $\delta_{l,u} = 0.69$ and 0.41. This shot is part of ν_* and β dimensionless confinement scaling studies of which more details can be found in Ref. 1. Linear runs using GYRO include kinetic electrons, deuterium and carbon ions, shear magnetic perturbations ($\delta B = \nabla \times \delta A_\parallel$), compressional magnetic perturbations ($\delta B_\parallel$), and electron pitch angle scattering. Geometric quantities are derived from numerical equilibrium reconstructions using LRDFIT (Ref. 47) that are constrained by external magnetic signals, diamagnetic flux, internal magnetic pitch angle (via E_R corrected MSE (Ref. 48)), toroidal rotation profiles ($Ma = v_{tor}/c_s \approx 0.5$ at the magnetic axis) measured from CHERS,[49] and an isotherm requirement [$T_e(R) \rightarrow T_e(\psi)$] using full profile Thomson scattering measurements.[50] Typical linear microtearing calculations use 24–32 radial grid points, 8 energies, 12 pitch angles, and 14 parallel orbit mesh points[43,44] (×2 signs of parallel velocity), as determined from extensive convergence studies.

Table I lists some of the equilibrium and plasma parameters at four radial locations $r/a = 0.5–0.8$ (where r is a half-diameter flux surface label) used in the following linear GYRO simulations. The local electron beta is defined as $\beta_e = 8\pi n_e T_e / B^2$ using the vacuum value $B_T = 0.35$ T. A second set of values $\beta_{e,unit}$ are defined replacing B_T with the quantity $B_{unit} = B_T \cdot \rho / r \cdot d\rho/dr$ [$\rho = (\Psi_t/\pi B_T)^{1/2}$ and Ψ_t is the toroidal flux] as used in normalizations throughout GYRO.

TABLE I. Equilibrium and plasma parameters used in the linear GYRO simulations for NSTX 120968 at t = 0.56 s.

r/a	q	s	T_e/T_i	a/L_{Te}	a/L_{Ti}	a/L_{ne}	a/L_{nd}	β_e (%)	$\beta_{e,unit}$ (%)	$\alpha_{p,unit}$	ν_{ei} (c_s/a)	Z_{eff}	γ_E (c_s/a)
0.5	1.36	0.81	1.02	1.88	2.64	−0.19	1.22	10.5	3.58	0.75	0.89	2.36	0.24
0.6	1.69	1.74	1.05	2.72	2.36	−0.83	0.35	8.84	2.45	0.60	1.45	2.92	0.17
0.7	2.47	3.26	0.97	3.05	1.96	−0.32	−1.21	7.03	1.35	0.56	2.81	2.83	0.12
0.8	4.00	3.68	0.88	2.94	1.95	2.79	3.46	4.79	0.56	1.24	4.34	2.79	0.09

The parameter $\alpha_{p,unit} = q^2 R_0 8\pi/B^2_{unit}\, dp/dr$ is a generalized MHD-α parameter.[45] The electron-ion collision frequency is determined by $\nu^{e/i} = Z_{eff}\cdot\nu_{ei}$, where $\nu_{ei} = 4\pi n_e e^4 \log\Lambda/(2T_e)^{3/2} m_e^{1/2}$ is defined using Z = 1 and, therefore, depends only on n_e and T_e. The E × B shear rate is given by $\gamma_E = -r/q\cdot d\omega_0/dr$,[44,51] where $\omega_0 = -d\Phi_0/d\psi$ is the toroidal rotation frequency, Φ_0 is the equilibrium electric field potential, and ψ is the poloidal flux (assuming no other contribution to E_r from diamagnetic or poloidal flows, which is appropriate for the core of most NSTX NBI plasmas). Other normalizing quantities are the minor radius, a = 0.62 m, sound speed $c_s = (T_e/m_d)^{1/2}$, and deuterium ion gyroradius evaluated at the local electron temperature, $\rho_{s,D} = (m_d\cdot T_e)^{1/2}/B_{unit}$.

Fig. 1 shows the real frequency and growth rate spectra for the four radial locations listed in Table I. Between r/a = 0.5–0.8, the microtearing mode is found to be the dominant ion scale instability, with real frequencies in the electron drift direction and growth rates that peak around $k_\theta\rho_s$ = 0.6–0.8. Using the local values of ρ_s and the definition of the poloidal wavenumber, $k_\theta = nq/r$, the range of unstable toroidal modes in this region of the plasma is n ≈ 5–70 ($k_\theta\rho_s \approx$ 0.05–1). The exception to this is at r/a = 0.7 where the microtearing modes are unstable at even higher wavenumbers up to $k_\theta\rho_s \le 5$. The real frequencies roughly follow the electron diamagnetic drift frequency, $\omega \approx \omega_{*e} = k_\theta\rho_s\cdot(a/L_{ne} + a/L_{Te})\cdot(c_s/a)$, at all locations.

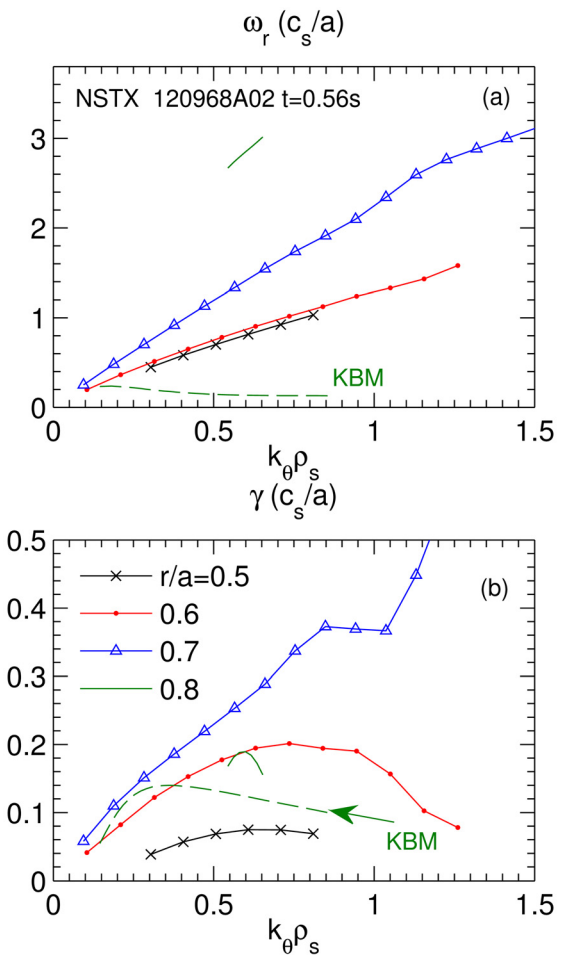

FIG. 1. (Color online) Real frequency and growth rate spectra for r/a = 0.5–0.8. Solid lines represent microtearing modes, while the dashed line represents kinetic ballooning modes calculated at r/a = 0.8 using the eigenvalue solver.

The ETG instability at higher $k_\theta\rho_s$ is found to be stable in this plasma, and no thermal gradient driven microinstability is predicted inside r/a < 0.45. The peak linear growth rates of the microtearing modes are on the order of the E × B shear rates listed in Table I, suggesting E × B shear suppression may become important in non-linear simulations (as initially found in Ref. 20.) Clearly, microtearing modes are prevalent throughout the gradient region r/a = 0.5–0.8 and likely play an important role in the core confinement of this and related plasmas.

At r/a = 0.8, the microtearing mode is dominant between $k_\theta\rho_s \approx$ 0.5–0.7, although outside of this range, a stronger mode appears with very small frequency. The GYRO eigenvalue solver is used to track this second root even when it becomes subdominant (dashed line). An additional scan in β_e (at $k_\theta\rho_s$ = 0.36, Fig. 2(a)) shows that the growth rate of this mode increases rapidly above a threshold of $\beta_e \approx 2.7\%$ and so we identify it as KBM. We note that, while the strong density gradient and large fraction of trapped particles (f_t = 59%) at r/a = 0.8 should contribute significantly to a TEM instability, the large collisionality ($\nu_e/\omega > 10$) is very stabilizing.

Tracking the KBM root in radial location (Fig. 2(b)), we find that it is unstable with an appreciable growth rate in the

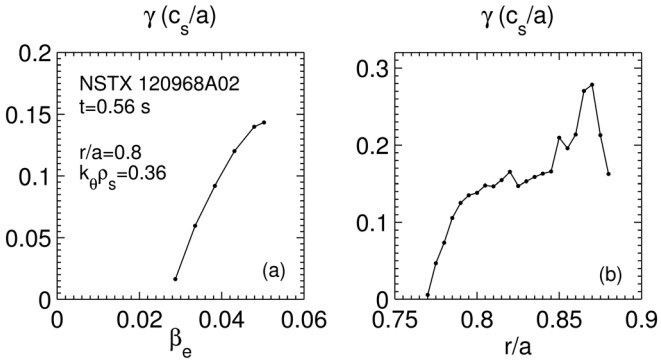

FIG. 2. (a) Linear KBM growth rate ($k_\theta\rho_s$ = 0.36) vs. (a) electron beta at r/a = 0.8 and (b) r/a.

range $r/a \approx 0.77$–0.88, suggesting it may be important towards the edge region of this plasma. (We do not track the KBM further out as the pedestal is approached and numerical resolution requirements become more stringent.) As we will see below, at $r/a = 0.8$, the KBM becomes important as both electron and deuterium density gradients are substantially larger ($a/L_{ne} = 2.8$ and $a/L_{nd} = 3.5$). This provides a high pressure gradient (characterized by the larger value of $\alpha_{p,unit}$ in Table I) which is the source of free energy for KBMs, while primarily only the electron temperature gradient drives microtearing modes. This will be clarified below through the use of parameter scans.

Fig. 3 shows the characteristic linear microtearing structure of electrostatic potential (φ), shear magnetic perturbation ($A_{\|}$), and parallel current perturbation ($j_{\|}$) for the most unstable microtearing modes at $r/a = 0.6$ and 0.8 plotted against the extended ballooning angle. The $A_{\|}$ perturbation is strongly ballooning ($|\theta| < \pi$ rad) and symmetric around the outboard midplane ($\theta = 0$) (even parity), giving a finite flux-surface-averaged resonant $\langle A_{\|} \rangle_{\theta}$ indicative of a tearing mode. In contrast to this, the potential is anti-symmetric (odd parity) and can extend a much larger distance along the field line, especially, in the $r/a = 0.6$ case. The parallel current is also extended very far along the field line, with significant amplitude out to $|\theta| > 40$ rad for $r/a = 0.6$. This broad parallel extent is consistent with a broad k_r spectra and consequent narrow current channel as the radial wavenumber is related to ballooning angle via $k_r = k_\theta s(\theta - \theta_0)$ (the ballooning parameter $\theta_0 = 0$ in these linear calculations). What physically determines the width of the potential and parallel current layers (and, therefore, the necessary radial resolution) in the tokamak microtearing mode is of great interest but left as a topic for future work.

Fig. 4 shows the real frequency and growth rate spectra at $r/a = 0.6$ using different physical model assumptions. The case of two ion species (deuterium and carbon, consistent with the experimental value of $Z_{eff} = 2.9$) is slightly more unstable than the case with only deuterium, with a broader spectra and a maximum growth rate ~15% larger. Compressional magnetic perturbations are much smaller than the shear magnetic perturbations responsible for the microtearing mode ($\delta B_{\|}/\delta B_{\|} \sim 1/50$). Neglecting them makes virtually no difference to the linear microtearing calculation, similar to MAST calculations.[16] However, they can influence the strength of other instabilities[45,52,53] (such as the KBM found above), and so we keep them in all calculations throughout this paper.

The equilibrium pressure gradient used when calculating local geometric quantities (e.g., ∇B drift)[44–46] includes the contribution of fast ions from beam heating, as calculated by

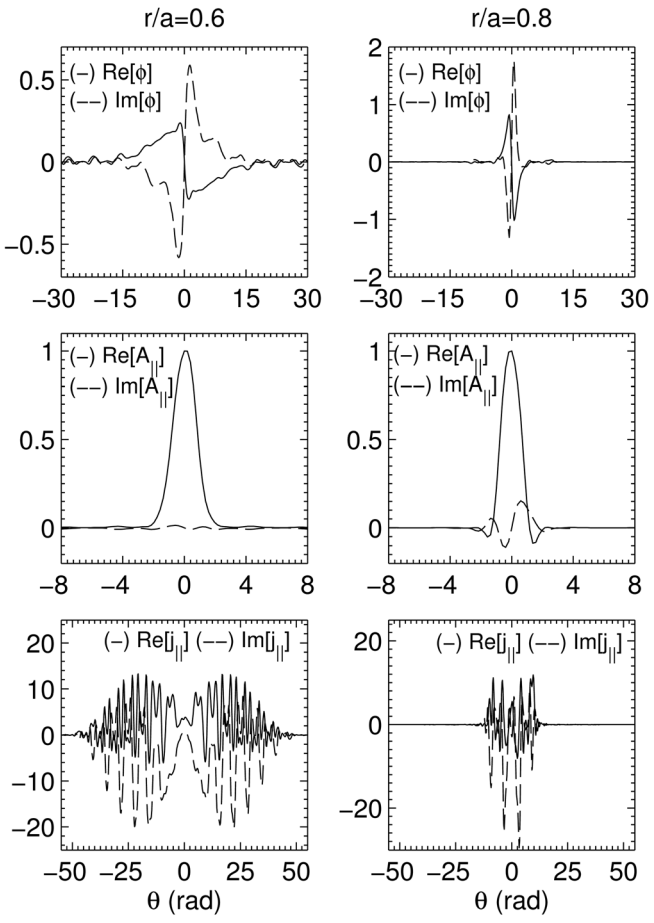

FIG. 3. φ, $A_{\|}$, and $j_{\|}$ microtearing eigenfunctions at $r/a = 0.6$ and 0.8 ($k_\theta \rho_s \approx 0.6$).

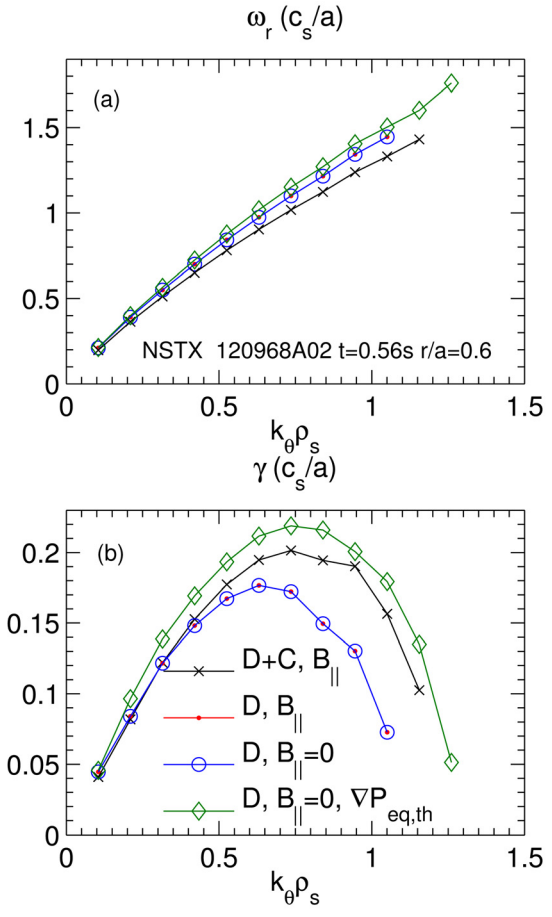

FIG. 4. (Color online) (a) Real frequency and (b) linear growth rate spectra at $r/a = 0.6$ for four different model assumptions: (black cross) two ions (D + C) with $B_{\|}$, (red dot) D only with $B_{\|}$, (blue circle) D only without $B_{\|}$, (green diamond) D only without $B_{\|}$, and thermal equilibrium pressure gradient.

the NUBEAM module in TRANSP.[54] On the $r/a = 0.6$ surface, the total normalized pressure gradient, $-a\nabla P 8\pi/B^2_{unit} = 0.14$, is 70% larger than that using only the thermal species. Using only the thermal contribution, $\nabla P_{eq,th}$, in a local expansion of the Grad-Shafranov equilibrium (Fig. 4, green diamonds), leads to a broadening of the unstable spectra to higher $k_\theta \rho_s$ and a ~25% increase in maximum linear growth rate. We consider this difference to represent an uncertainty estimate as a result of not self-consistently including the fast ion profile in the equilibrium reconstruction.

While adding a significant contribution to the total pressure gradient, the fast ion density is very small at $r/a = 0.6$ ($n_{fast}/n_e = 3.6 \times 10^{-3}$) and an additional linear run at one wavenumber (using an extremely small time step to satisfy the CFL limit for the energetic ions, $T_{i,fast}/T_e = 70$) shows it has negligible impact on the linear growth rate. It is, therefore, justified to neglect fast ions as a dynamic species, but we keep their contribution in the total equilibrium pressure gradient, which is held fixed throughout the paper regardless of ion species composition and plasma gradients.

III. PARAMETER SCANS

Having found the microtearing mode to be important in the region $r/a = 0.5$–0.8, we now vary parameters individually to determine how it scales based around this experimental operation point. The results of this study will be used to help discriminate the microtearing mode from scaling behavior of other micro-instabilities such as ETG, TEM, and KBM. It also provides a baseline for comparison with nonlinear simulations.[20,40]

A. Collisionality

One of the most distinguishing features of the microtearing mode is the fact that the growth rate peaks at some finite value of electron collisionality. An example is shown in Fig. 5 for the case of $r/a = 0.6$, where the peak happens to occur very near the local experimental value (square symbol). As ν_{ei} is reduced, the microtearing mode growth rate is reduced. This scaling trend is qualitatively consistent with the global energy confinement trends, $B\tau_E \sim \nu_*^{-0.95}$ observed in NSTX analysis.[1] (Similar results have also been found in MAST.[3]) This behavior is unique compared to traditional electrostatic drift wave instabilities where increasing collisionality ($\nu_e > 0$) tends to provide a *stabilizing* influence to trapped electrons which otherwise enhance the ITG, TEM, and ETG instabilities in the collisionless limit ($\nu_e = 0$). As shown in Fig. 5, as ν_{ei} is increased further, the linear growth rates are again reduced. This peaking behavior is generally predicted to occur in slab theory, regardless of whether the time-dependent thermal force[23,26–28] or trapped particle effects[33] are responsible and depends on the ratio of $Z_{eff}\cdot\nu_{ei}/\omega$. For the calculations in Fig. 5, the peak occurs for $Z_{eff}\cdot\nu_{ei}/\omega \sim 4$, which falls in the range of early slab calculations $Z_{eff}\cdot\nu_{ei}/\omega \sim 1$–$10$.[27,28]

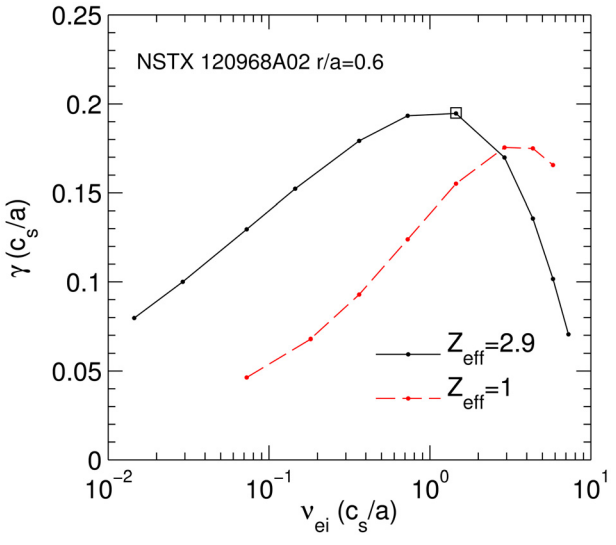

FIG. 5. (Color online) Linear growth rates verses ν_{ei} (defined using $Z_i = 1$). Square symbol represents the experimental value.

Fig. 5 shows a second scan where the carbon impurity density is set to zero, $n_c = 0$ ($Z_{eff} = 1$), which leads to two distinct effects. First, reducing Z_{eff} reduces the electron-ion collision frequency, $\nu^{e/i} = Z_{eff}\cdot\nu_{ei}$, so that when plotted vs ν_{ei} (defined for $Z = 1$), the peak growth rate is shifted to the right, verifying that it is the total e-i collision frequency that determines the peak in the growth rate. Second, the reduced ionic charge leads to a smaller shielding of the electrostatic potential as follows. Because of the narrow potential structures ($k_r\rho_s > 1$, corresponding to the extended eigenfunctions in Fig. 3), the ion response is almost perfectly unmagnetized, or adiabatic, so that $\delta n_i/n_i \approx -Z_{eff}\cdot\delta\varphi/T_i$. As Z_{eff} is reduced, potential perturbations become stronger (relative to $\delta A_\parallel$), which in this case provides a stabilizing effect. The overall result is that for experimental values of collisionality, reducing Z_{eff} provides a stabilizing influence to the microtearing mode. The fact that larger φ perturbations are stabilizing is opposite to the predictions in both slab[27] and MAST (Ref. 16) calculations in which stabilization occurred when artificially suppressing φ to zero. The reason for this difference is unclear but is presumably related to the influence of $\nabla\varphi$ on $E_\parallel$ as discussed in Ref. 24.

The same collisionality scan was performed at four radial locations, as shown in Fig. 6 ($k_\theta\rho_s \approx 0.6$). At all locations, the scaling of the microtearing mode is qualitatively similar to the results above. However, we find that the local experimental value of ν_{ei} can reside above that of the peak growth rate such that reducing collisionality leads to increasing γ. This nonmonotonic dependence of growth rate with ν_{ei} complicates the simple interpretation of the global confinement scaling mentioned above. Determining where this peak occurs (which varies between $Z_{eff}\cdot\nu_{ei}/\omega = 1$–$4$ for the cases in Fig. 6) and if the non-linear transport follows the same trend is of great interest for experimental interpretation of the confinement scaling.

Fig. 6 also shows that a different mode becomes dominant at $r/a = 0.5$ and 0.8 when collisionality is reduced about an order of magnitude from the values in this high-ν_* discharge. Additional scans in β_e at these lower values of ν_{ei} identify these modes as hybrid ITG/KBM modes, similar to those identified in the collisionless limit in a different NSTX discharge.[45]

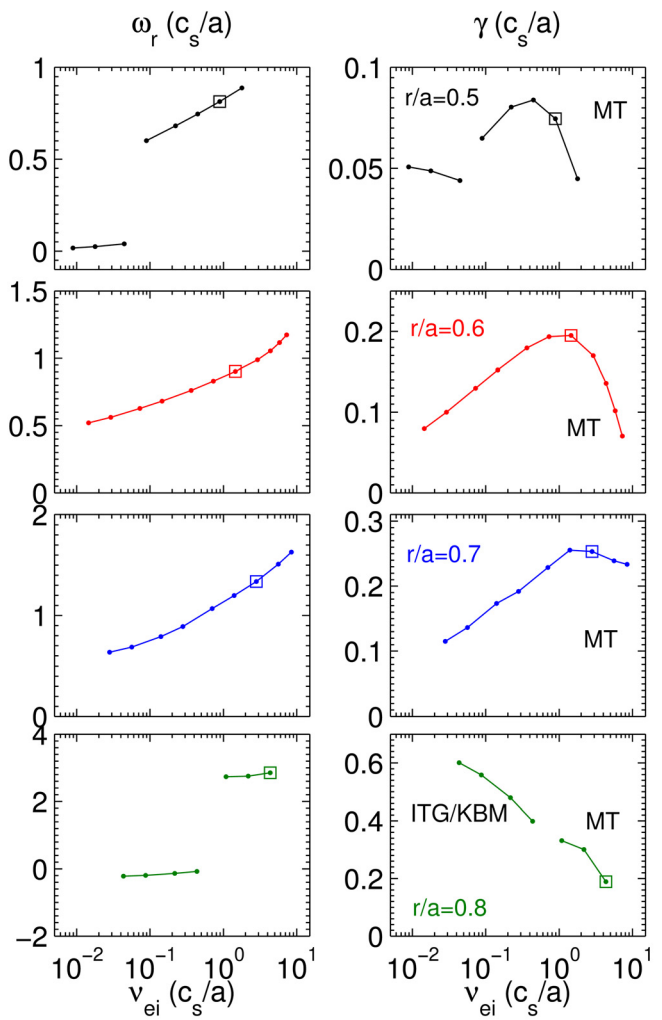

FIG. 6. (Color online) Real frequency (left) and growth rate (right) for $k_\theta\rho_s \approx 0.6$ vs. ν_{ei} at four radial locations ($r/a = 0.5$–0.8). Square symbols represent experimental values.

B. Temperature gradient

All microtearing theory and previous gyrokinetic calculations indicate that it is the electron temperature gradient responsible for instability and we find the same to hold true for these NSTX cases. Fig. 7 shows the frequency and growth rate spectrum at $r/a = 0.6$ as a/L_{Te} is varied between 0.75–1.5× the experimental value. As the temperature gradient is increased, the real frequencies track ω_{*e} and the wavenumber of the peak growth rate increases between $k_\theta\rho_s \approx 0.45$–$0.75$. There is a clear threshold behavior as expected from the simple theoretical arguments and observed in previous simulations.[16,18,39–41] In the case of $r/a = 0.6$, we find $(a/L_{Te})_{crit,MT} \approx 1.4$ to be about half the experimental value, $a/L_{Te,exp} = 2.73$.

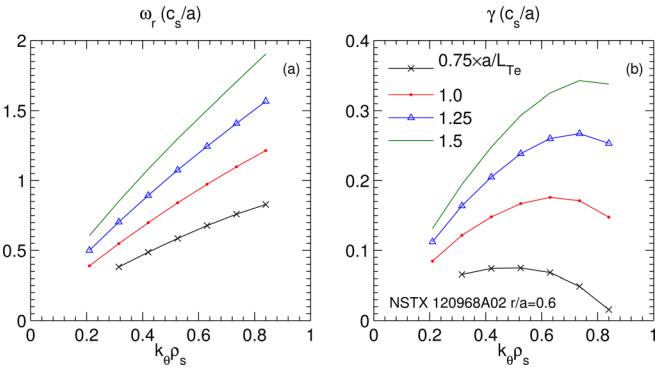

FIG. 7. (Color online) Linear microtearing growth rates vs $k_\theta\rho_s$ for varying normalized electron temperature gradient at $r/a = 0.6$.

Similar scans have been performed for the other radial locations in Table I. Fig. 8 summarizes the results by comparing the inferred threshold gradient with the local experimental values. In this high-ν_* discharge, the experimental gradients are 2–3 times larger than the linear microtearing threshold between $r/a = 0.5$–0.8.

We re-iterate that the electron scale ($k_\theta\rho_s \gg 1$) ETG instability is predicted to be stable in this plasma with threshold gradients much larger than experimental values ($a/L_{Te,etg} \sim 5$–8). This is primarily a consequence of the relatively large values of Z_{eff} (2.4–2.9) as the linear ETG threshold gradient is proportional to $a/L_{Te,crit} = (1 + Z_{eff}T_e/T_i)\cdot(\cdots)$ in the absence of a strong density gradient.[36] As noted above, reducing Z_{eff} can be stabilizing to microtearing modes, therefore, varying Z_{eff} may be a potentially useful experimental knob to discriminate between ETG or microtearing behavior in NSTX.

C. Density gradient

To test the influence of varying density gradient, we scale all species gradients (electron, deuterium, and carbon) by the same factor to maintain quasi-neutrality, $\Sigma_s(Z_s\cdot a/L_{ns}) = 0$, and plot the results against the electron density gradient, a/L_{ne}. A number of interesting features arise for such a scan as shown in Fig. 9. For small variations around the experimental values (squares), we find the growth rate can either increase with a/L_{ne} ($r/a = 0.6$), as reported in the case of ASDEX-UG edge parameters,[39] or decrease ($r/a = 0.8$). Over a broader range there is, however, a well-

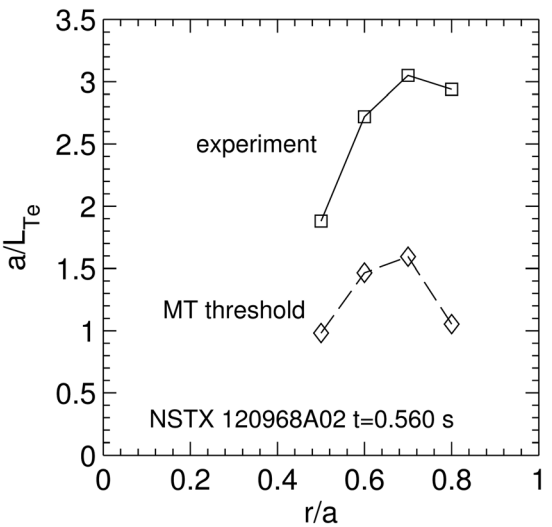

FIG. 8. Normalized electron temperature gradient from experiment and linear microtearing thresholds ($k_\theta\rho_s < 1$).

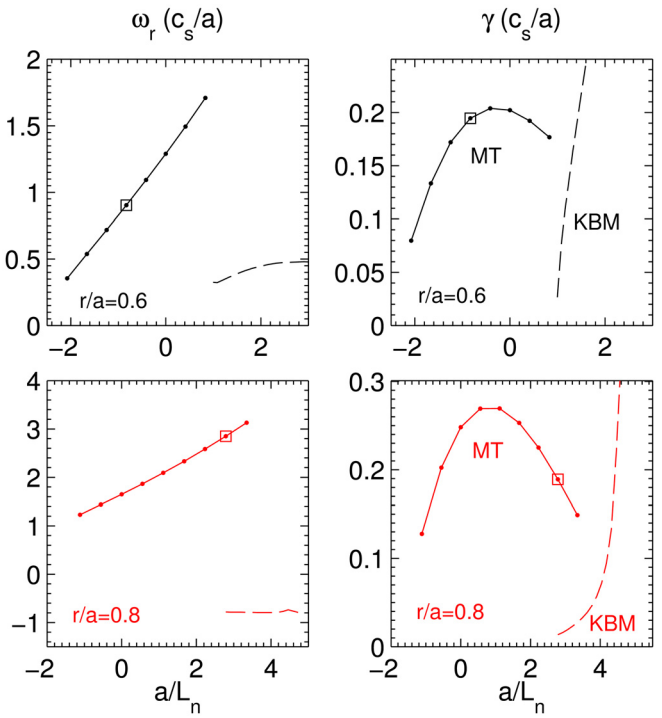

FIG. 9. (Color online) Real frequency and linear growth rate ($k_\theta\rho_s \approx 0.6$) vs. normalized density gradient for both $r/a = 0.6$ and 0.8. Square symbols represent experimental values. Dashed lines are kinetic ballooning modes.

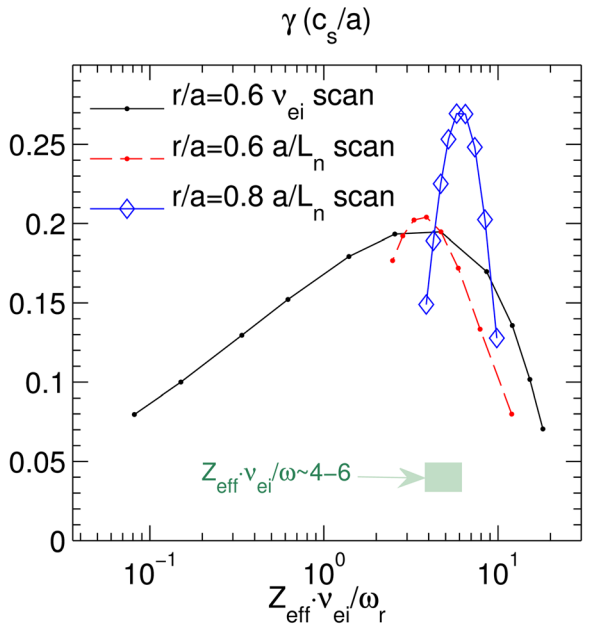

FIG. 10. (Color online) Linear growth rates vs. $Z_{eff}\cdot\nu_{ei}/\omega_r$ for ν_{ei} and a/L_n scans.

defined peak at $a/L_{ne} = -0.5$ and $+0.8$ for $r/a = 0.6$ and 0.8, respectively.

As a/L_{ne} becomes larger, a different instability eventually overcomes the microtearing mode. Using the eigensolver, we identify this instability as the kinetic ballooning mode (peaking at $k_\theta\rho_s \approx 0.15$ for $r/a = 0.6$ and $k_\theta\rho_s \approx 0.35$ for $r/a = 0.8$), as it is very sensitive to increases in a/L_{ne} above a finite threshold. This sharp threshold behavior is similar to that found when increasing β_e for the base parameters at $r/a = 0.8$ shown in Fig. 2(a).

Because the real frequencies track the electron diamagnetic frequency, ω_{*e}, the non-monotonic dependence of the growth rate on a/L_n can, at least partially, be related to the fact that it varies the ratio of $Z_{eff}\cdot\nu_{ei}/\omega$. Fig. 10 shows the linear growth rates plotted against this ratio for the scans shown in Figs. 5 and 9. The peak growth rates occur around $Z_{eff}\cdot\nu_{ei}/\omega \approx 4$–6 for these cases falling in the same range as that found in the sheared slab calculations. While this ratio provides a rough estimate of where in collisionality the microtearing mode is most unstable, very large magnitudes of density gradient (positive or negative) must also contribute an additional stabilizing influence. As shown in Fig. 10, the growth rates fall dramatically as a/L_n is varied, greatly narrowing the range in $Z_{eff}\cdot\nu_{ei}/\omega$ in which they are significant. For the core confinement region in many NSTX plasmas, the density profile is nearly flat so little stabilization is expected from density gradients.

D. Electron beta

The microtearing mode is fundamentally electromagnetic in nature and both analytic theory and earlier gyrokinetic simulations demonstrate that finite electron beta is critical for the existence of instability. Fig. 11 illustrates this result (at $k_\theta\rho_s \approx 0.6$) for this NSTX high-$\nu_*$ discharge. Extrapolating the curves in Fig. 11, the threshold is found to be $\beta_{e,crit} \approx [5.0, 3.0, 2.0, 1.7]\%$ at $r/a = [0.5, 0.6\ 0.7, 0.8]$, about 2–3× smaller than the local experimental values. Well above the threshold, in the range of the experimental values (squares), the growth rates increase moderately with β_e, eventually becoming invariant for much larger values. The moderate destabilization with β_e in the experimental range is qualitatively consistent with the weak confinement scaling $\Omega\tau_E \sim \beta^{-0.1}$ observed in NSTX.[1]

As microtearing growth rates do not increase indefinitely with β_e, eventually, the kinetic ballooning mode will be important. For wavenumbers near the peak in the microtearing spectrum ($k_\theta\rho_s \geq 0.6$), KBM often does not become dominant until β_e reaches values 2–10× larger than experiment. However, as shown in Fig. 1 (at $r/a = 0.8$), the KBM spectrum often peaks at much lower wavenumbers, between $k_\theta\rho_s = 0.15$–0.35 for $r/a = 0.5$–0.8. Tracking the KBM root at these wavenumbers, we find that the KBM can overcome microtearing growth rates between ~1.5–2.5× the experimental values. Practically, these are substantially larger than expected experimental values. However, if the microtearing mode is stabilized, e.g., by reducing collisionality, we might expect the KBM (or hybrid ITG/KBM) to eventually become important in the core confinement region.

E. Safety factor and magnetic shear

Previous gyrokinetic studies have not investigated the influence of safety factor and magnetic shear on the stability of microtearing modes. We can isolate the dependence on q and s by using a local equilibrium expansion[46,55] for the $r/a = 0.6$ surface, including κ and δ shape moments and equilibrium pressure gradient but enforcing up-down

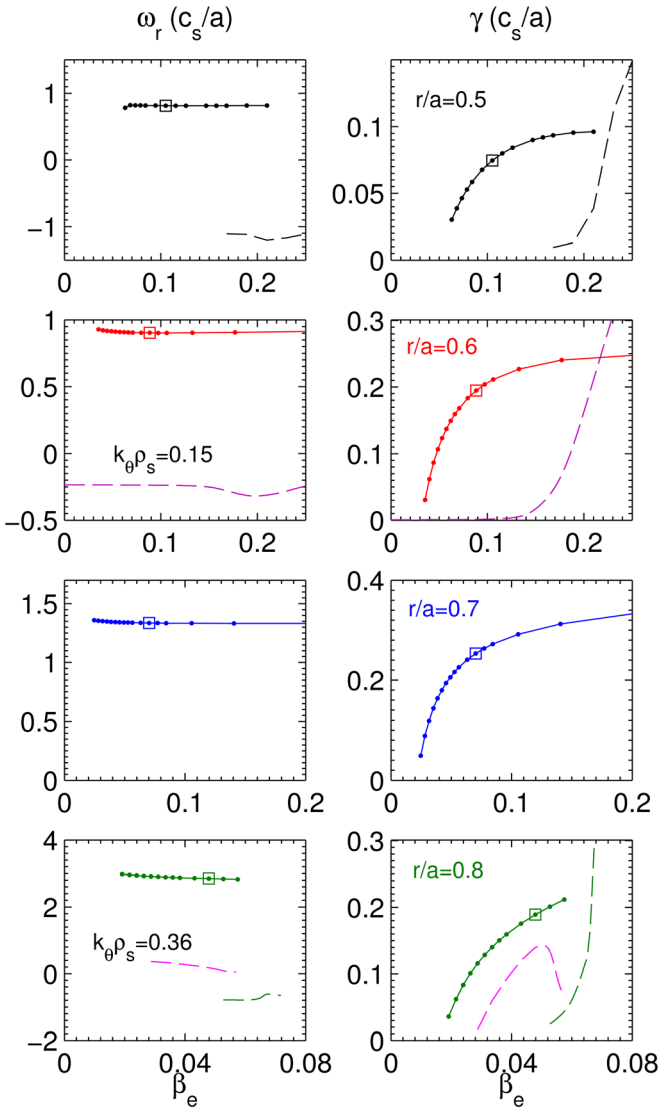

FIG. 11. (Color online) Microtearing growth rates ($k_\theta\rho_s \approx 0.6$) vs electron beta. Dashed lines are kinetic ballooning modes. Square symbols represent experimental values.

symmetry. This approximation is justifiable for the baseline parameters as there is good agreement compared to the general equilibrium case. From this starting point, we independently vary safety factor and magnetic shear. Fig. 12(a) shows

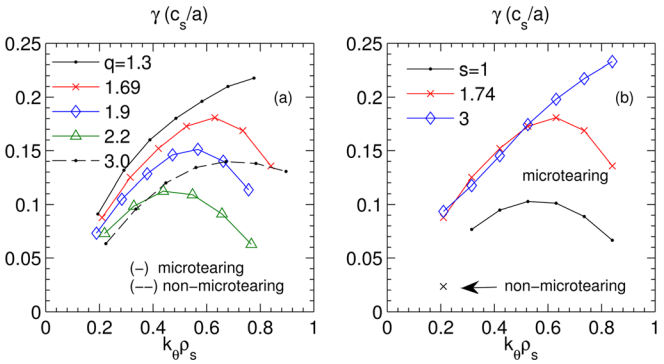

FIG. 12. (Color online) Linear growth rates varying (a) q and (b) s, using local equilibrium expansion for $r/a = 0.6$. Experimental values are $q = 1.69$ and $s = 1.74$.

that increasing q is stabilizing over a range of $q = 1.3$–2.2 around the experimental values at $r/a = 0.6$, while Fig. 12(b) show that increasing s between 1–3 is destabilizing and also appears to ultimately broaden the unstable spectra. In either case, at sufficiently low s or high q, the microtearing mode becomes weak enough that a different instability with non-tearing parity enters the spectra.

Focusing on one wavenumber ($k_\theta\rho_s = 0.63$) at $r/a = 0.6$, we see a number of interesting features arise for finer scans in s and q (Fig. 13). First, for larger values of magnetic shear, the growth rates are eventually reduced, opposite to the trend discussed above, so there is a local maximum around $s \approx 3$. Second, as magnetic shear is reduced, we find a separate instability in a narrow range of $s \approx 0.25$–0.8 (which appears at lower k_θ at $s = 1$ in Fig. 12). These modes exhibit non-tearing parity but do not behave like KBMs as there is no apparent threshold in β_e. The growth rate at $s = 0.3$ increases mostly with increasing ∇T_e, ∇n, and ν_{ei}. Finally, for very small positive or negative values of magnetic shear, $|s| \sim 0$, the microtearing mode becomes strongly unstable with a local maximum around zero shear.

The dramatic increase of growth rates for near zero shear is contradictory to some previous calculations for NSTX NBI discharges where weak/negative shear was found to be stabilizing.[17,19] On the other hand, microtearing modes were found to be unstable near zero shear in at least one NSTX L-mode case at ion scales[11] and also more recently at electron scales ($k_\theta\rho_s = 3$–20) for near zero shear closer to the magnetic axis ($r/a < 0.5$) in RF heated plasmas.[37] For our case at $s = -0.05$, the mode is unstable over a

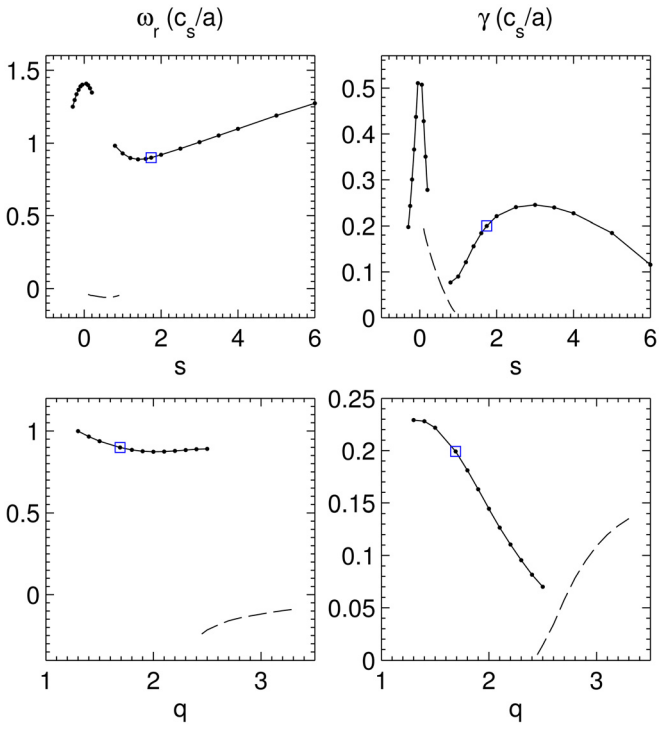

FIG. 13. (Color online) Real frequency and growth rate for varying magnetic shear (s) and safety factor (q). Square symbols represent experimental values. Solid lines are microtearing and dashed lines are non-tearing parity.

much narrower range $k_\theta \rho_s < 2$, so not obviously the same flavor of instability as the electron scale version.

The local peak in growth rate around $s = 3$ is actually consistent with that observed in sheared slab calculations,[27] which is explained by the following. In slab theory, a damping rate due to fieldline bending in the narrow inner layer can be shown to be proportional to $\Delta'/L_s \sim \Delta' \cdot s/qR$. In the high-m limit applicable to microtearing modes, the tearing parameter is negative, $\Delta' = -2\ k_\theta$ ($k_\theta = m/r$), such that growth rates are reduced at increasing s. This accounts for the behavior above $s > 3$. However, this damping rate was derived using the "constant-ψ" assumption, i.e., $d/dx(A_\parallel)$ is allowed to be discontinuous over the inner region while $A_\parallel$ (or ψ) is assumed to be constant. As shown in Ref. 27 and observed in our toroidal calculations, as magnetic shear is reduced, the $A_\parallel$ mode structure begins to vary more substantially around the tearing layer and the constant-ψ approximation is no longer valid. This leads to additional field line bending stabilization and the corresponding decrease in growth rates at lower shear ($s < 3$). Based on considerations of the inner layer width and $dA_\parallel/dx$ (deteremined from $j_\parallel$), Gladd *et al.*[27] provide a simple estimate of when the constant-ψ approximation is valid, $(R/L_{Te})^2 (q/s)^2 \beta_e \ll 1$. Using the parameters in Table I, for $r/a = 0.5$–0.8, we find this parameter is always near unity (0.9–2.4) violating the condition for validity and consistent with the mode being stabilized with reduced shear.

As noted above, the inverse shear length in the slab limit can be expressed in toroidal geometry as $1/L_s = s/qR$. Therefore, the stabilization at increased q (shown in Fig. 13 for the experimental value $s = 1.74$) is analogous to reducing magnetic shear in the range $s = 0.8$–3. To emphasize this point, we plot the growth rates from both scans against the ratio s/q in Fig. 14. Generally, in the range of $s/q = 0.5$–1.5, which covers the region of $r/a = 0.5$–0.8 in the high-ν_* plasma, we expect increasing s/q to be destabilizing. This scaling is opposite to that expected for the toroidal ETG instability (for similar values of s and q), whose stability

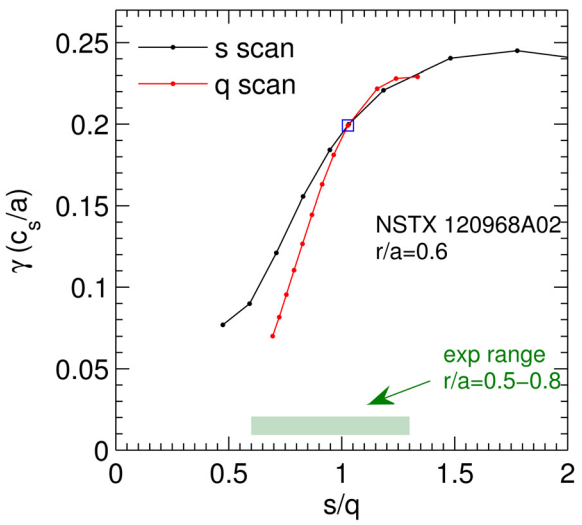

FIG. 14. (Color online) Growth rate vs. the ratio s/q for $r/a = 0.6$. Square symbol represents experimental value at $r/a = 0.6$. Also shown by the shaded region is the range of s/q over the region $r/a = 0.5$–0.8.

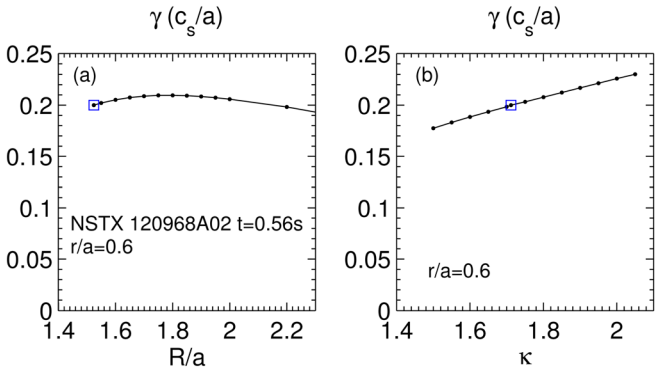

FIG. 15. (Color online) Variation of growth rate ($k_\theta \rho_s = 0.63$) as aspect ratio (R/a) and elongation (κ) is varied locally for the $r/a = 0.6$ surface. Square symbols represent experimental values.

threshold increases with s/q in the form $(R/L_{Te})_{crit} \sim (1.3 + 1.9 \cdot s/q)$[36] (for $s > 0$). This difference may provide an additional opportunity to experimentally distinguish microtearing and ETG electron transport in spherical tokamaks.

F. Aspect ratio and elongation

Because of engineering constraints, plasmas in the proposed NSTX-Upgrade[56,57] will operate at slightly higher aspect ratio and elongation. Using the local equilibrium expansion, we perform two final scans varying both R/a and κ on the $r/a = 0.6$ surface to investigate their isolated influence on the microtearing mode. As shown in Fig. 15, the growth rates ($k_\theta \rho_s = 0.63$) are very weakly dependent on these two quantities. Of course, these scans are not truly representative of reality as they are not derived from self-consistent global equilibrium solutions. We expect that any significant change to microtearing modes in scenarios with higher R/a and κ will come predominantly through corresponding changes in q, s, β_e, and ν_e.

IV. DISCUSSION AND SUMMARY

Detailed linear microstability analyses have been performed using physically comprehensive gyrokinetic simulations based on measured parameters and equilibrium reconstruction in a single high-ν_* NSTX discharge that is part of a broader energy confinement scaling study.[1] The microtearing mode is found to be unstable over a significant region of the plasma between $r/a = 0.5$–0.8. Numerous parametric scans have been employed to investigate how the mode scales. The results provide some intuition on the physical nature of the mode, when and where it may be expected to be unstable, and how it might be discriminated from other instabilities such as ETG or KBM modes.

For the parameters studied in this paper, the microtearing mode is clearly an electromagnetic drift-tearing mode that requires sufficient electron collisionality, beta, and temperature gradient to be driven unstable, with real frequencies that follow the electron diamagnetic drift frequencies, $\omega \sim \omega_{*e} = k_\theta \rho_s (a/L_n + a/L_{Te}) \cdot (c_s/a)$. The mode is insensitive to compressional magnetic perturbations and the ion response is nearly unmagnetized, or adiabatic, so that $\delta n_i/n_i$

$\approx -Z_{eff}\cdot\delta\varphi/T_i$. As impurity concentration and Z_{eff} are increased, electrostatic perturbations are shielded through the adiabatic response, which in some cases provides a destabilizing influence.

One of the distinguishing features of the microtearing mode is the non-monotonic dependence of the growth rate with collisionality. Most relevant is the ratio of electron-ion collision frequency to mode frequency, $Z_{eff}\cdot\nu_{ei}/\omega$, where ν_{ei} is defined for $Z=1$ to explicitly track the dependence on Z_{eff}. For both ν_{ei} and a/L_n scans at different radii and Z_{eff}, we find the local maximum to occur in the range $Z_{eff}\cdot\nu_{ei}/\omega\sim 1$–6, similar to that found for sheared slab calculations (1–10).[27,28] This range is rather broad in the context of experimental interpretation and a more precise prediction of the local maximum would be beneficial in the context of understanding transport and confinement scaling.

A new result highlighted in this paper is the non-monotonic dependence of microtearing growth rate on magnetic shear through the ratio s/q, which is related to field-line bending as shown in slab theory.[27] While reduced at very large values ($s/q>2$), around the experimental values ($s/q=0.6$–1.3 in the region $r/a=0.5$–0.8), microtearing growth rates increase with s/q. This trend is opposite to ETG scaling for similar values and provides an additional opportunity to distinguish these two modes experimentally. For values of magnetic shear near zero, this simple interpretation is not guaranteed to be accurate. We also find microtearing growth rates to be reduced by increases in the equilibrium pressure gradient (e.g., by fast ions) and relatively insensitive to isolated changes in aspect ratio or elongation.

Another identifying feature of the microtearing mode is the threshold-like behavior with both a/L_{Te} and β_e. Varying β_e, we find the threshold to be 2–3× smaller than the experimental β_e values in the range of $r/a=0.5$–0.8. Alternatively, the experimental temperature gradient exceeds the a/L_{Te} threshold by 2–4. In contrast, the ETG instability is found to be stable, largely attributable to the higher values of $Z_{eff}=2.4$–2.9. Given the different dependence of each mode on effective ionic charge (through both electron-ion collisions and potential shielding), we suggest that varying Z_{eff} could help distinguish the effects of these two modes experimentally.

Noting the stiff nature of non-linear microtearing transport[20,40] with a/L_{Te}, it would be useful to develop an expression for the scaling of the threshold gradient. Such an expression was determined from the slab calculations in Refs. 27 and 28, $R/L_{Te}\sim(Z_{eff}\hat{\nu}_{ei}sa/\beta_e qR)^{1/2}$. While this form qualitatively captures the expected scaling with beta and collisionality (above the local maximum in $Z_{eff}\cdot\nu_{ei}/\omega$), it has the opposite trend in s/q for the values relevant to this high-ν_* discharge. Future calculations will focus on developing a similar expression useful for NBI-heated ST discharges.

It is interesting to note that the kinetic ballooning mode (or hybrid ITG/KBM (Ref. 45)) often appeared throughout our analysis. For instance, at $r/a=0.8$, the peak KBM growth rate is almost as strong as the microtearing mode. The balance between these two is influenced significantly by a strong conventional density gradient ($\nabla n_e<0$ and $a/L_{ne}>0$) that is destabilizing to KBM (through β') while stabilizing to MT. We also found that the KBM can become dominant at both lower ν_e (as microtearing is stabilized) and higher β_e. The linear KBM spectrum peaks at lower wavenumber than the microtearing modes found in NSTX ($k_\theta\rho_s\sim 0.15$–0.35 compared to $k_\theta\rho_s>0.6$) so non-linear simulations will be required to determine which dominates in a saturated turbulence state when they have comparable linear growth rates.

Many of the features and scaling of these NSTX microtearing modes appear to be reproduced by slab theory and calculations. We conclude by highlighting a few of the key missing elements in microtearing theory that, if accounted for, might provide a more complete unifying treatment of the instability in tokamaks. First, the influence of a strongly ballooning $A_\parallel$ is unclear as no parallel variation is allowed for in any of the analytic theories. Second, there is no direct inclusion of toroidal effects beyond ad hoc particle trapping.[33–35] For STs at large $\varepsilon=a/R$, these theories are severely restricted to a small region in collisionality ($\varepsilon\omega<\nu_e<\omega$) inconsistent with the broad range of parameters studied in this paper. Third, it is unclear how to relate the microtearing mode at finite positive shear ($s=0.5$–5) to that found at near-zero-shear ($|s|\sim 0$), both at ion scales ($k_\theta\rho_s<2$) in the high-ν_* NBI discharge (and a separate case reported in Ref. 11), or at electron scales ($k_\theta\rho_s=3$–15) found in the core of RF heated discharges.[37] Finally, it would be useful to resolve why stronger electrostatic potential perturbations provide a stabilizing influence in this NSTX case, yet are destabilizing in both sheared slab[27] and MAST (Ref. 16) simulations. If this behavior changes with other parameters, it should influence how impurity concentration and ionic charge (Z_{eff}) influences the microtearing mode.

ACKNOWLEDGMENTS

We acknowledge useful discussions with S. P. Gerhardt, J. E. Menard, D. R. Mikkelsen, J. L. Peterson, and Y. Ren. This work was supported by DOE Contract Nos. DE-AC02–09CH11466, DE-FG03–95ER54309, and DE-AC52–07NA27344.

[1]S. M. Kaye, F. M. Levinton, D. Stutman, K. Tritz, H. Yuh, M. G. Bell, R. E. Bell, C. W. Domier, D. Gates, W. Horton, J. Kim, B. P. LeBlanc, N. C. Luhmann, Jr., R. Maingi, E. Mazzucato, J. E. Menard, D. Mikkelsen, D. Mueller, H. Park, G. Rewoldt, S. A. Sabbagh, D. R. Smith, and W. Wang, Nucl. Fusion **47**, 499 (2007).
[2]S. M. Kaye, R. E. Bell, D. Gates, B. P. LeBlanc, F. M. Levinton, J. E. Menard, D. Mueller, G. Rewoldt, S. A. Sabbagh, W. Wang, and H. Yuh, Phys. Rev. Lett. **98**, 175002 (2007).
[3]M. Valovič, R. Akers, M. de Bock, J. McCone, L. Garzotti, C. Michael, G. Naylor, A. Patel, C. M. Roach, R. Scannell, M. Turnyanskiy, M. Wisse, W. Guttenfelder, J. Candy, and the MAST team, Nucl. Fusion **51**, 073045 (2011).
[4]M. Valovič, R. Akers, G. Cunningham, L. Garzotti, B. Lloyd, D. Muir, A. Patel, D. Taylor, M. Turnyanskiy, M. Walsh, and the MAST team, Nucl. Fusion **49**, 075016 (2009).
[5]E. J. Doyle, Nucl. Fusion **47**, S18 (2007).
[6]C. C. Petty, Phys. Plasmas **15**, 080501 (2008).
[7]M. Kotschenreuther, W. Dorland, Q. P. Liu, M. C. Zarnstorff, R. L. Miller, and Y. R. Lin-Liu, Nucl. Fusion **40**, 677 (2000).
[8]H. R. Wilson, J.-W. Ahn, R. J. Akers, D. Applegate, R. A. Cairns, J. P. Christiansen, J. W. Connor, G. Counsell, A. Dnestrovskij, W. D. Dorland, M. J. Hole, N. Joiner, A. Kirk, P. J. Knight, C. N. Lashmore-Davies, K. G.

McClements, D. E. McGregor, M. R. O'Brien, C. M. Roach, S. Tsaun, and G. M. Voss, Nucl. Fusion **44**, 917 (2004).
[9]M. H. Redi, W. Dorland, R. Bell, P. Banoli, C. Bourdelle, J. Candy, D. Ernst, C. Fiore, D. Gates, G. Hammett, K. Hill, S. Kaye, B. LeBlanc, J. Menard, D. Mikkelsen, G. Rewoldt, J. Rice, R. Waltz, S. Wukitch, in *Proceedings of 30st EPS Conference on Controlled Fusion and Plasma Physics (St. Petersburg)* (2003), p. 4.94.
[10]M. H. Redi, S. Kaye, W. Dorland, R. Bell, C. Bourdelle, S. Ethier, D. Gates, G. Hammett, K. Hill, B. LeBlanc, D. McCune, J. Menard, D. Mikkelsen, G. Rewoldt, and E. Synakowski, in *Proceedings of 31st EPS Conference on Controlled Fusion and Plasma Physics (London)* (2004), p. 2.162.
[11]M. H. Redi, W. Dorland, C. L. Fiore, D. Stutman, J. A. Baumgaertel, B. Davis, S. M. Kaye, D. C. McCune, J. Menard, G. Rewoldt, in *Proceedings of 32nd EPS Conf. on Controlled Fusion and Plasma Physics (Tarragona)* (2005), p. 5.041.
[12]D. J. Applegate, C. M. Roach, S. C. Cowley, W. D. Dorland, N. Joiner, R. J. Akers, N. J. Conway, A. R. Field, A. Patel, M. Valovic, and M. J. Walsh, Phys. Plasmas **11**, 5085 (2004).
[13]C. M. Roach, D. J. Applegate, J. W. Connor, S. C. Cowley, W. D. Dorland, R. J. Hastie, N. Joiner, S. Saarelma, A. A. Schekochihin, R. J. Akers, C. Brickly, A. R. Field, M. Valovic, and the MAST team, Plasma Phys. Controlled Fusion **47**, B233 (2005).
[14]J. W. Connor, C. M. Roach, R. J. Hastie, P. Helander, T. J. Martin, D. J. Applegate, N. Joiner, M. Reshko, S. Saarelma, W. D. Dorland, S. C. Cowley, S. Newton, and A. R. Field, in *Proceedings of the IAEA-FEC, TH/P2–2* (2006).
[15]D. Applegate, Ph.D. thesis, Imperial College London, 2006.
[16]D. J. Applegate, C. M. Roach, J. W. Connor, S. C. Cowley, W. Dorland, R. J. Hastie, and N. Joiner, Plasma Phys. Controlled Fusion **49**, 1113 (2007).
[17]F. M. Levinton, H. Yuh, M. G. Bell, R. E. Bell, L. Delgado-Aparicio, M. Finkenthal, E. D. Fredrickson, D. A. Gates, S. M. Kaye, B. P. LeBlanc, R. Maingi, J. E. Menard, D. Mikkelsen, D. Mueller, R. Raman, G. Rewoldt, S. A. Sabbagh, D. Stutman, K. Tritz, and W. Wang, Phys. Plasmas **14**, 056119 (2007).
[18]K. L. Wong, S. Kaye, D. R. Mikkelsen, J. A. Krommes, K. Hill, R. Bell, and B. LeBlanc, Phys. Rev. Lett. **99**, 135003 (2007).
[19]K. L. Wong, S. Kaye, D. R. Mikkelsen, J. A. Krommes, K. Hill, R. Bell, and B. LeBlanc, Phys. Plasmas **15**, 056108 (2008).
[20]W. Guttenfelder, J. Candy, S. M. Kaye, W. M. Nevins, E. Wang, R. E. Bell, G. W. Hammett, B. P. LeBlanc, D. R. Mikkelsen, and H. Yuh, Phys. Rev. Lett. **106**, 155004 (2011).
[21]H. P. Furth, J. Killen, and M. N. Rosenbluth, Phys. Fluids **6**, 459 (1963).
[22]H. P. Furth, P. H. Rutherford, and H. Selberg, Phys. Fluids **16**, 1054 (1973).
[23]R. D. Hazeltine, D. Dobrott, and T. S. Wang, Phys. Fluids **18**, 1778 (1975).
[24]J. F. Drake and Y. C. Lee, Phys. Fluids **20**, 1341 (1977).
[25]J. F. Drake, N. T. Gladd, C. S. Liu, and C. L. Chang, Phys. Rev. Lett. **44**, 994 (1980).
[26]M. Rosenberg, R. R. Dominguez, W. Pfeiffer, and R. E. Waltz, Phys. Fluids **23**, 2022 (1980).
[27]N. T. Gladd, J. F. Drake, C. L. Chang, and C. S. Liu, Phys. Fluids **23**, 1182 (1980).
[28]D. A. D'Ippolito, Y. C. Lee, and J. F. Drake, Phys. Fluids **23**, 771 (1980).
[29]R. R. Dominguez, M. Rosenberg, and C. S. Chang, Phys. Fluids **24**, 472 (1981).
[30]C. S. Chang, R. R. Dominguez, and R. D. Hazeltine, Phys. Fluids **24**, 1655 (1981).
[31]A.B. Hassam, Phys. Fluids **23**, 2493 (1980).
[32]A. B. Hassam, Phys. Fluids **23**, 2493 (1980).
[33]L. Chen, P. H. Rutherford, and W. M. Tang, Phys. Rev. Lett. **39**, 460 (1977).
[34]P. J. Catto and M. N. Rosenbluth, Phys. Fluids **24**, 243 (1981).
[35]J. W. Connor, S. C. Cowley, and R. J. Hastie, Plasma Phys. Controlled Fusion **32**, 799 (1990).
[36]F. Jenko, W. Dorland, and G. W. Hammett, Phys. Plasmas **9**, 4096 (2001).
[37]D. R. Smith, W. Guttenfelder, B. P. LeBlanc, and D. R. Mikkelsen, Plasma Phys. Controlled Fusion **53**, 035013 (2011).
[38]L. Vermare, C. Angioni, A. Bottino, A. G. Peeters, and the ASDEX Upgrade Team, J. Phys.: Conf. Ser. **123**, 012040 (2008).
[39]D. Told, F. Jenko, P. Xanthopoulous, L. D. Horton, E. Wolfrum, and ASDEX Upgrade Team, Phys. Plasmas **15**, 102306 (2008).
[40]H. Doerk, F. Jenko, M. J. Pueschel, and D. R. Hatch, Phys. Rev. Lett. **102**, 155003 (2011).
[41]I. Predebon, F. Sattin, M. Veranda, D. Bonfiglio, and S. Cappello, Phys. Rev. Lett. **105**, 195001 (2010).
[42]J. Candy and R. E. Waltz, Phys. Rev. Lett. **91**, 045001 (2003).
[43]J. Candy and R. E. Waltz, J. Comput. Phys. **186**, 545 (2003).
[44]J. Candy and E. Belli, General Atomics Technical Report No. GA-A26818, 2010.
[45]E. A. Belli and J. Candy, Phys. Plasmas **17**, 112314 (2010).
[46]J. Candy, Plasma Phys. Controlled Fusion **51**, 105009 (2009).
[47]J. E. Menard, R. E. Bell, D. A. Gates, S. M. Kaye, B. P. LeBlanc, F. M. Levinton, S. S. Medley, S. A. Sabbagh, D. Stutman, K. Tritz, and H. Yuh, Phys. Rev. Lett. **97**, 095002 (2006); http:/w3.pppl.gov/~jmenard/software/lrdfit/lrdfit-index.htm.
[48]F. M. Levinton and H. Yuh, Rev. Sci. Instrum. **79**, 10F522 (2008).
[49]R. E. Bell and R. Feder, Rev. Sci. Instrum. **81**, 10D724 (2010).
[50]B. P. LeBlanc, R. E. Bell, D. W. Johnson, D. E. Hoffman, D. C. Long, and R. W. Palladino, Rev. Sci. Instrum. **74**, 1659 (2003).
[51]R. E. Waltz and R. L. Miller, Phys. Plasmas **6**, 4265 (1999).
[52]C. Bourdelle, W. Dorland, X. Garbet, G. W. Hammett, M. Kotschenreuther, G. Rewoldt, and E. J. Synakowski, Phys. Plasmas **10**, 2881 (2003).
[53]N. Joiner, A. Hirose, and W. Dorland, Phys. Plasmas **17**, 072104 (2010).
[54]R. J. Hawryluk, in *Proceedings of Course on Physics of Plasmas Close to Thermonuclear Conditions (Varenna)* (1979), Vol 1, p. 19.
[55]R. L. Miller, M. S. Chu, J. M. Greene, Y. R. Lin-liu, and R. E. Waltz, Phys. Plasmas **5**, 973 (1998).
[56]J. E. Menard, M. Bell, J. Bialek, J. Canik, J. Chrzanowski, M. Denault, L. Dudek, D. A. Gates, S. Gerhardt, W. Guttenfelder, R. Hatcher, R. Kaita, S. Kaye, C. Kessel, E. Kolemen, H. Kugel, R. Maingi, M. Mardenfeld, D. Mueller, B. Nelson, C. Neumeyer, M. Ono, E. Perry, R. Ramakrishnan, R. Raman, S. Sabbagh, M. Smith, V. Soukhanovskii, T. Stevenson, R. Strykowsky, P. Titus, K. Tresemer, M. Viola, M. Williams, R. Woolley, A. Zolfaghari, and the NSTX Team, "Overview of the physics and engineering design of NSTX Upgrade," Nucl. Fusion (submitted).
[57]S. P. Gerhardt, D. A. Gates, S. M. Kaye, R. Maingi, J. E. Menard, S. A. Sabbagh, V. Soukhanovskii, M. G. Bell, R. E. Bell, J. M. Canik, E. Fredrickson, R. Kaita, E. Kolemen, H. Kugel, B. P. LeBlanc, D. Mastrovito, D. Mueller, and H. Yuh, Nucl. Fusion **51**, 073031 (2011).